Available online at www.sciencedirect.com

ScienceDirect

IFAC PapersOnline CONFERENCE PAPER ARCHIVE

IFAC PapersOnLine 55-6 (2022) 563–568

Fault Detection and Isolation Based on Deep Learning for a Fresnel Collector Field

Sara Ruiz-Moreno * **Antonio J. Gallego** * **Adolfo J. Sanchez** ** **Eduardo F. Camacho** *

* *Dept. de Ingeniería de Sistemas y Automática, University of Seville, Camino de los Descubrimientos, no number E-41092, Seville, Spain (email: srmoreno@us.es, agallego2@us.es, efcamacho@us.es)*

** *Dept. of Mechanical, Biomedical and Manufacturing Engineering, Munster Technological University, Cork T12 P928, Ireland (email: adolfo.j.sanchez@ieee.org)*

Abstract:
With the advancement of new technologies, power systems are increasingly equipped with more sensors and actuators, heightening the risk of failure. This fact, together with the vulnerability of solar plants –not only to internal faults but also to the action of the sun, rain, wind, and animals, among others– gives rise to the need for detecting and identifying faults to deal with them. Methods that detect and diagnose faults play a crucial role in solar plants, allowing the systems to cope with them as soon as they occur and before they lead to large-scale problems. This work proposes using neural networks to detect and distinguish mirror and flow rate faults in a Fresnel plant. In addition, a defocusing stage is added to access hard-to-isolate faults, increasing the accuracy of 89.61% to 97.43%. These results contribute to the problem of isolability in thermal solar plants. The simulations for obtaining the neural networks and the results were conducted on a model of the Fresnel plant located at the Engineering School of Seville, Spain (ETSI).

Keywords: Fresnel, Artificial Intelligence, Fault Detection, Fault Diagnosis, Solar Energy

1. INTRODUCTION

In the second half of the seventies, there was an impulse to use renewable energy sources due to the oil crisis. Currently, its use has remained due to the growing environmental awareness in developed countries (Camacho et al., 2014; Goswami et al., 2000). Solar energy is the most important one among renewable energy sources since it is the most abundant. Another advantage of solar energy is the possibility of using thermal storage systems to stock the exceeding thermal energy and respond to short-term high load demands when it is needed (Islam et al., 2018).

Some applications of solar energy are the production of electric power or supply of air conditioning. The interest in the second application is increasing and especially important in areas exposed to high solar radiation (Kim and Infante Ferreira, 2008). This work focuses on Fresnel collectors, a type of solar thermal power system composed of thin mirror strips that concentrate the incoming solar irradiance onto a tube placed at the focal line. This tube contains a heat transfer fluid (HTF) that heats up as sunlight hits it. Compared to parabolic trough collectors, these plants possess different advantages, notably lower cost and more straightforward design. In this work, a model of a Fresnel collector belonging to a solar cooling plant of the Engineering School of Seville, Spain (ETSI, Escuela Técnica Superior de Ingeniería) is used (Bermejo et al., 2010).

Research in Fresnel collector plant technologies and control is increasing and attracting growing attention. An example of this is the work carried out by Whitheephanich et al. (2013), where model predictive control (MPC) is applied for temperature tracking. Gallego et al. (2020) compares an adaptive MPC strategy to a PID with feedforward using an unscented Kalman filter as a state estimator. Concerning the design of these plants, Rungasamy et al. (2021) reviews the methodologies and mechanisms for optical loss, and Pulido-Iparraguirre et al. (2019) presents an optically optimized design with geometrical modifications for obtaining homogeneous thermal power along the year.

As research and technologies evolve, these plants add more sensors and actuators, and the more components there are, the more probability of faults occurring. A fault is an unpermitted deviation of one or more features in a plant that conduces to undesired behaviors. To acknowledge the existence of faults and start mitigation or repair actions, fault detection (FD) techniques arise. Moreover, once a fault is detected, it is helpful to determine the location and type of a fault. This process is called fault isolation (FI). Fault detection and isolation (FDI) is included in the group of fault detection and diagnosis (FDD) techniques.

FDD techniques are applied in many fields. Specifically, in the power systems area it is a topic of great interest. Pillai et al. (2019) studies and compares the different

⋆ This research was supported by the European Union's Horizon 2020 research and innovation program under the ERC Advanced Grant agreement No 789051.

10.1016/j.ifacol.2022.07.188

fault detection methods for photovoltaic plants. Regarding wind turbines, Qu et al. (2021) proposes the use of neural networks with a technique based on improved triplet loss to detect various types of faults. Freire et al. (2020) proposes a predictive control strategy combined with FDI to adjust system control in case of faults in microgrids.

The work presented by Faure et al. (2016) reviews the failure modes, effects, and subsystems reliability in solar thermal systems, and a methodology to analyze the impact of faults is proposed by Faure et al. (2018). Most recent applications of FDI to thermal solar energy focus on the detection stage or on isolation in the whole field rather than the collectors. Zahra et al. (2020) uses a fuzzy observer for FD in a solar power field, simplifying the collectors as a whole faulty subsystem. A similar simplification is made by Kalogirou et al. (2008), who uses neural networks to predict temperatures and determine if a fault is located at the collectors or the pipe that connects them to the storage system. Correa-Jullian et al. (2020) predicts data of a solar hot water system using a neural network to obtain residuals and detect faults, and the method presented by Jiang et al. (2019) detects and classifies faults in solar water heaters combining support vector machines and D-S evidence theory.

The main contribution of this work is the use of a methodology to detect and isolate faults in a Fresnel plant using machine learning combined with a defocus strategy. The neural network is used to detect faults and classify them into two main locations, and the defocusing is used to augment the accuracy of the neural network, dealing with the difficulty of distinguishing the type of fault on certain occasions

The paper is organized as follows. Section 2 gives a description of the system, presenting the Fresnel plant used for making the experiments, the equations for modeling it, and the controller. Next, section 3 describes the methodology applied, and the experimental results are presented in section 4. Finally, sections 5 and 6 extract some discussion and conclusions from the work.

2. SYSTEM DESCRIPTION

In this section, the solar collector field and its mathematical model are presented. These kinds of systems are described using two types of models: the concentrated parameter model and the distributed parameter model. In this work, the distributed parameter model is used for simulation purposes, and the concentrated parameter model is used for obtaining the controller and during the fault isolation process. These equations are similar to those of the parabolic trough plants. The difference lies in the computation of the shade factor and the geometrical efficiency.

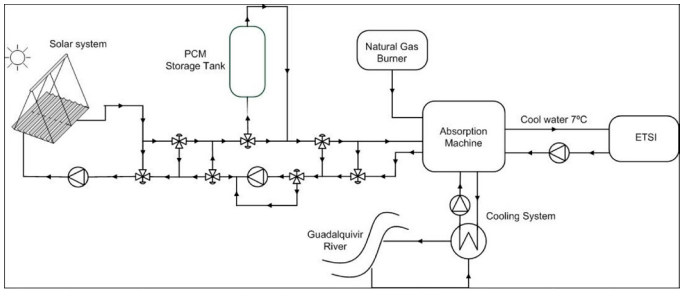

Fig. 1. General scheme of the Fresnel plant at ETSI.

The solar plant modeled in this work is installed on the roof of the Engineering School of Seville (ETSI). It consists of a Fresnel collector field, a phase change materials (PCM) storage tank, an auxiliary power system, and a double-effect absorption chiller, as shown in figure 1. The solar field is composed of 11 rows of linear Fresnel collectors with a total reflective surface of 352 m^2, see figure 2. The sunlight is reflected on a 64 m long metal pipe containing the heat transfer fluid (HTF). This tube, called a receiver, is enclosed by a secondary reflector. It consists of a metal cover with a mirror to reflect the radiation part that has not impacted directly on the receiver. The HTF is heat pressurized water that is then delivered to the water absorption chiller. A more detailed description can be found in Robledo et al. (2011); Gallego et al. (2019).

Fig. 2. Fresnel collector field at ETSI.

2.1 Distributed Parameter Model

The distributed parameter model is represented by equations 1 and 2, which describe the energy balances in the metal and the fluid with spatially distributed variables, with the subscripts m and f referring to metal and fluid, respectively, and the notation given by table 1. The faults are modeled as multiplicators $\alpha_{K_{opt}}$ and α_q.

$$\rho_m C_m A_m \frac{\partial T_m}{\partial t} = \alpha_{K_{opt}} I K_{opt} n_o G + \\ -H_l G(T_m - T_a) - L H_t (T_m - T_f) \quad (1)$$

$$\rho_f C_f A_f \frac{\partial T_f}{\partial t} + \alpha_q \rho_f C_f q \frac{\partial T_f}{\partial x} = L H_t (T_m - T_f) \quad (2)$$

The equations are solved by dividing the tube into 64 segments of 1 m long and using an integration time of 0.25 s. The density, specific heat, and heat transmission coefficient are obtained as the segment temperature and flow rate functions.

$$\rho_f = -0.0025 T_f^2 - 0.203 T_f + 1003.91 \quad (3)$$

$$C_f = 5.16 \cdot 10^{-7} T_f^4 - 7.78 \cdot 10^{-2} T f^3 + 18.73 T_f^2 \quad (4)$$

Table 1. Parameters and variables description.

Symbol	Description	Units
t	Time	s
A	Cross-sectional Area	m^2
G	Collector aperture	m
L	Pipe length	m
A_f	Transversal area of the interior pipe	m^2
$I(t)$	Direct solar irradiance	W/m^2
$q(t)$	Flow rate	l/s
$T_a(t)$	Ambient temperature	°C
$T(t,x)$	Temperature	°C
$C(t,T)$	Specific heat capacity	J/(kg °C)
$\rho(t,T)$	Density	kg/m^3
$H_l(t,T)$	Thermal loss coefficient	$W/(m^2$ °C)
K_{opt}	Optical efficiency	–
$n_o(t)$	Geometric efficiency	–
$H_t(t,T)$	Metal-fluid heat transmission coefficient	$W/(m^2$ °C)

$$H_t = q^{0.8}(1.34 \cdot 10^{-4} T_f^4 - 7.78 \cdot 10^{-2} T_f^3 + \\ +18.73 T_f^2 - 2.57 \cdot 10^3 T_f + 4.11 \cdot 10^5) \quad (5)$$

$$H_l = 9.2782 \cdot 10^{-4} \left(T_f - T_a\right) - 1.8 \cdot 10^{-3} \quad (6)$$

The computation of the geometric efficiency uses a 2D and a 3D model of the plant and contains complex trigonometrical functions, as well explained by Robledo et al. (2011). It is formed by the shade factor and the incidence angle of the solar beam.

2.2 Concentrated Parameter Model

The concentrated parameter model –or lumped parameter model– provides a general description of the field and is used for control and fault isolation purposes. Equation 7 describes the internal energy variation of the fluid.

$$C\frac{dT_{out}}{dt} = \alpha_{K_{opt}} n_o K_{opt} S I + \\ -\alpha_q q P_{cp}(T_{out} - T_{in}) - H_l S(T_{mean} - T_a) \quad (7)$$

where C is the thermal capacity, $P_{cp} = \rho_m C_m$, *in*, *out* and *mean* refer to inlet, outlet and mean values between them, and the reflective surface S is 352 m^2.

2.3 Flow Control

The controller used in this work is a simple feed-forward for reference temperature tracking, manipulating the flow rate of the HTF. The controller is implemented using the concentrated parameter model as in equation 8 and has a sample time of 30 s.

$$q(t) = \frac{n_o K_{opt} S I - H_l(T_{mean} - T_a)}{P_{cp}(T_{ref} - T_{in})} \quad (8)$$

3. METHODOLOGY APPLIED

The approach of this work is mainly based on the use of artificial neural networks to detect and isolate faults in real-time. The faults that affect a Fresnel collector can be grouped into two main categories: those related to the mirrors and their reflectivity and faults in the flow rate. The first group is associated with corrosion, breakage, coating, and degradation of the collectors due to dirt or external elements, while the second group of faults is due to flowmeter and flow rate errors. Note that the first group also includes pyrheliometer faults, as I and K_{opt} always act jointly on the system forming a product. This method does not consider temperature measurement faults, which can be analyzed independently and are an object of future inclusion. Although the considered plant only has one line of reflectors, the methodology is extendable to bigger plants and can be applied to each line independently, as the faults are analyzed in the collector area, not considering the pump. This allows the detection of flow imbalances.

In many cases, it is not easy to distinguish one type of failure from another as, for example, a temperature drop could be due to a dirty collector, but also to a misreading of the flow rate. To solve this problem, we propose a decoupling stage in which the collectors are defocused, and the flow rate is decoupled from the reflectivity and collector efficiency.

3.1 Artificial Neural Networks

An artificial neural network (ANN) is a model that can approximate every nonlinear function by emulating the functioning of the human brain. It is composed of neurons that are generally arranged in layers (McCulloch and Pitts, 1943). Currently, their use is widespread, with applications in many different fields, from industrial systems to business, as well as medicine or art, among others, and is a growing line of study (Abiodun et al., 2018).

This work uses multilayer perceptrons, a type of feedforward neural network (Fine, 2006). Each neuron computes a linear regression problem and has an activation function that transforms the data. The weights are obtained with backpropagation (Rumelhart et al., 1986; Lillicrap et al., 2020) using the partial derivatives of the output error. In this work, the ANNs are trained using scaled conjugate gradient backpropagation, which performs a search along the conjugate directions giving a faster convergence. Before training the ANN, a suitable dataset is obtained, scaled between -1 and 1 and divided into the training set, the validation set, and the test set. The outputs are labeled using one-hot encoding.

The inputs to the neural network are selected to be the same that the concentrated parameter model uses: T_{in}, T_{out}, dT_{out}/dt, T_a, I, the assumed q and n_0.

Neural networks are trained in a trial-and-error process. The parameters and architecture are selected and the ANN is trained. The whole process is repeated until obtaining the desired accuracy. Then, to validate the results, the confusion matrix, accuracy and F1-score are obtained.

- Accuracy: hit rate. It takes account of the true positives (TP) and true negatives (TN) over the sum of true positives, true negatives, false positives (FP), and false negatives (FN).

$$Acc = \frac{TP + TN}{TP + TN + FP + FN} \quad (9)$$

- Confusion matrix: it allows the visualization of the number of instances that were assigned to each class.

		Real	
		Positive	Negative
Predicted	Positive	TP	FP
	Negative	FN	TN

- F1-score: the harmonic mean of precision and recall.

$$F1 = 2 \cdot \frac{Pre \cdot Rec}{Pre + Rec} \tag{10}$$

- Precision: the rate of correct TP over all positive-assigned instances.

$$Pre = \frac{TP}{TP + FP} \tag{11}$$

- Recall: the rate of correct TP over all positives.

$$Rec = \frac{TP}{TP + FN} \tag{12}$$

3.2 Defocusing

The defocusing mechanism consists of modifying the angle of incidence of the solar rays on the mirrors reducing the efficiency. It is used in commercial plants to prevent the HTF temperature from being too high, improving performance and protecting plant components (Alhaj and Al-Ghamdi, 2018; Sánchez et al., 2020).

This work proposes to use a defocusing strategy to isolate faults. As this entails an energy waste during the time the analysis is performed, it will only be used when the output of the neural network is not clear–that is, when the output values corresponding to the two types of failure are very similar.

When the collector is defocused, the faults in its efficiency stop affecting the system, so it is possible to isolate the faults. An estimate of the flow rate multiplicator is used as a residual, obtained from the concentrated parameter model. Whenever this value differs from 1 in a band of 5% above and below, it is considered that a fault has been detected.

$$\hat{\alpha_q} = -\frac{1}{qP_{cp}(T_{out} - T_{in})} \cdot \left(C\frac{dT_{out}}{dt} + H_l S(T_{mean} - T_a)\right) \tag{13}$$

4. EXPERIMENTAL RESULTS

This section shows the results obtained when simulating the system under different conditions. First, some simulations were carried out to create the dataset for training the neural network, and then, different simulations were performed to validate its behavior in execution time.

The neural networks were trained using a dataset containing 1799514 instances obtained from simulations with different types of faults. Constant irradiances from 700 W/m^2 to 1000 W/m^2, constant inlet temperatures between 85 ºC and 160 ºC, and constant temperature references from 4 ºC to 20 ºC above the inlet temperature were used. Multiplicative faults between 0.1 and 0.9 for the collectors and additive negative and positive faults between ±5 m^3/h and ±0.5 m^3/h were added. The faults were considered to occur before the start of each day. The dataset was divided into training (70%), validation (15%), and test (15%) subsets.

Different neural networks were trained. Table 2 shows the accuracies obtained with each one of the subsets. The column "Neurons" indicates the number of nodes in each hidden layer of the ANN. The selected ANN is the one with 200 neurons in the first hidden layer, 100 neurons in the second one, and 50 neurons in the third one, as it obtained the best results under the data from the dataset. All trained neural networks showed an excellent ability to maintain accuracy among the three subsets.

Table 2. Accuracies of the neural networks in the dataset.

Neurons	Acc train (%)	Acc valid. (%)	Acc test (%)
49	83.9	83.9	83.8
49-21	91.1	90.9	91.1
49-21-9	87.0	87.1	86.9
100-50	91.8	91.8	91.7
100-50-20	92.4	92.4	92.3
200-100	93.0	92.9	93.0
200-100-50	**94.3**	**94.2**	**94.2**
400-200	91.5	91.5	91.4

At the output of the neural networks, a low-pass filter with a time constant of 1 hour is added. It prevents false alarms due to variations in the plant. The alarms are activated when some neural network output corresponding to a fault is higher than 75%. For the mode with the defocusing strategy, the alarms are directly activated if the sum of the outputs not corresponding to the predicted class is lower than 10%. Otherwise, the output will be considered unclear, and the defocusing stage will begin. An alarm will be given when the residual value exceeds 5%.

To validate the behavior of the neural network, one-day simulations were performed with different values of temperatures and faults. The faults appear at different times during the simulation. The irradiance profiles correspond to days with low dynamics, and their highest points vary between around 700 W/m^2 and 1000 W/m^2. Table 3 contains the confusion matrix without applying the defocusing step, and the confusion matrix of the simulations with the defocusing stage is shown in table 4. Table 5 gathers and compares the F1-scores and accuracies of each mode.

		Real		
		Faultless	K_{opt}	q
Predict.	Faultless	324	0	0
	K_{opt}	0	280	57
	q	0	44	267

Table 3. Confusion matrix for the normal mode.

		Real		
		Faultless	K_{opt}	q
Predict.	Faultless	324	0	0
	K_{opt}	0	304	4
	q	0	20	320

Table 4. Confusion matrix for the mode with defocusing.

Figures 3 and 4 show the results obtained after a 0.9 fault occurs at 14:00 in the efficiency of the collector (10% loss of efficiency). The output of the neural network is clear enough to determine the existence of the fault correctly.

Mode	F1-score (%)			Acc (%)
	Faultless	K_{opt} fault	q fault	
Normal	100.0	84.72	84.09	89.61
With defocussing	100.0	96.04	96.24	97.43

Table 5. Accuracies and F1-scores.

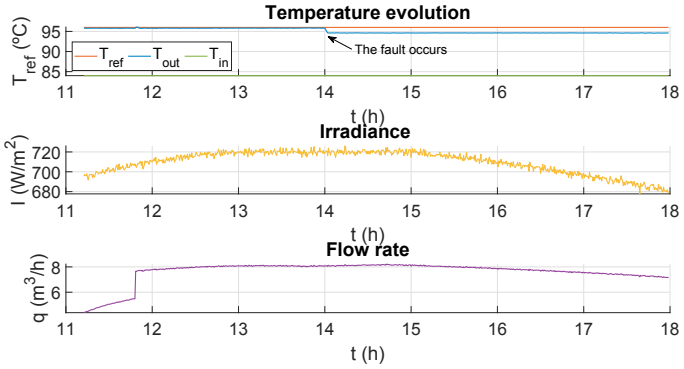

Fig. 3. Temperatures, irradiance and flow rate evolution from the first experiment with a fault of 0.9 in the efficiency of the collector after hour 14:00.

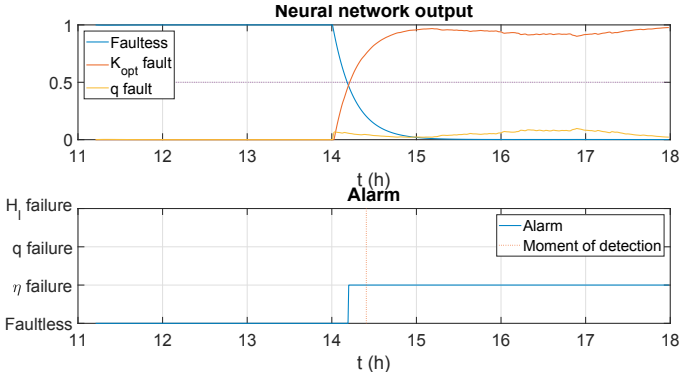

Fig. 4. Neural network output from the first experiment with a fault of 0.9 in the efficiency of the collector after hour 14:00.

Figures 5 and 6 show a case in which the defocusing strategy was activated. Although it has not been possible to conduct experiments at the plant because it is currently not operational, the irradiance profile was obtained from the sensor in the real plant. In this experiment, there was a +2.5 m^3/h fault at 13:00 in the flow rate, but the ANN could not provide a clear output. The collector was defocused, causing a drop in temperature and an increase in the output of the neural network corresponding to the efficiency of the collector during several minutes. The residual estimated a deviation of around 0.4 points in the multiplicator.

5. DISCUSSION

This section aims to discuss the results obtained from the work and shown above. The neural network was trained and tested under different circumstances, obtaining an accuracy of 89.61%. Afterward, a decoupling stage was implemented to improve the neural network results by defocusing the collector. The accuracy obtained was 97.43%. From these results, it stands out that it is possible to train a neural network for detecting faults and distinguishing between two main locations with high accuracy.

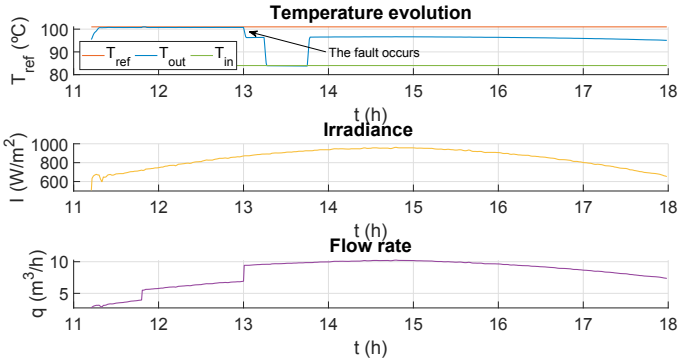

Fig. 5. Temperatures, irradiance and flow rate evolution from the second experiment with +2.5 m^3/h fault after hour 13:00.

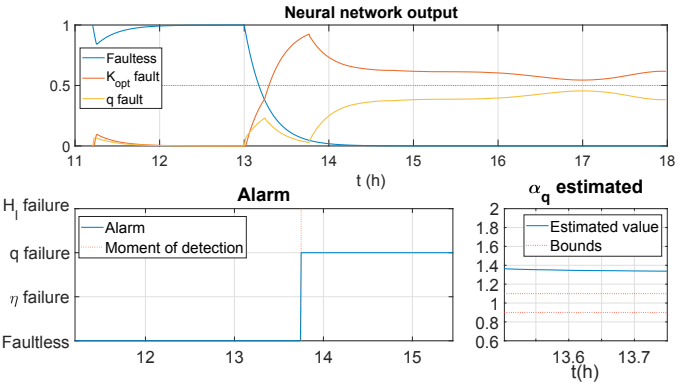

Fig. 6. Neural network output from the second experiment with +2.5 m^3/h fault after hour 13:00.

Results improve significantly with the decoupling strategy. Although it is costly to implement because it involves defocusing a collector to obtain residuals that do not depend on the reflectivity, its application will not be frequent: the probability of failure is compounded by the probability that the ANN will struggle to detect it. Furthermore, the band from which this method is applied can be modified. Currently, it is applied when the nonselected class output is over 10%, but this value may be increased. It is a compromise between the frequency of hits and the frequency of time desired to defocus. Although the method is not directly considering the existence of multiple faults, it is implicitly taken into account since one of two simultaneous faults will be detected and, as soon as it is repaired, the other will be alarmed too.

6. CONCLUSIONS

This paper has described a methodology for detecting faults and isolating them into two classes: faults in the collectors related to their reflectivity and efficiency and faults in the flow rate related to errors in the flowmeter. A neural network is used as a first classifier and, if the output is not clear, a defocusing stage is added to decouple the efficiency of the collectors and improve the performance. The results show an accuracy improvement of almost 8%. This study provides the foundation for an FDD strategy in Fresnel solar plants.

In this work, days with low dynamics are considered, with smooth changes in the irradiance along the day. Future

research will assess the applicability of the methodology under extreme conditions, with large clouds passing by. Furthermore, other issues to address will be to perform a complete FDD scheme by analyzing the magnitude of the fault, and to implement fault-tolerant control techniques.

The work was carried out by simulation. For applying the methodology to a real plant, it will be necessary to reduce the data size with a deeper analysis of the amount of data needed and the probability of some of the considered magnitude of faults. Moreover, commercial plants have more lines and collect more data per day. For reproducing this experiment without data reduction, the ETSI Fresnel plant would require 8 years, Liddell (NREL, 2022a) would require 2 years and Puerto Errado 2 (NREL, 2022b) would need 4 months.

REFERENCES

Abiodun, O.I., Jantan, A., Omolara, A.E., Dada, K.V., Mohamed, N.A., and Arshad, H. (2018). State-of-the-art in artificial neural network applications: A survey. *Heliyon*, 4(11), e00938.

Alhaj, M. and Al-Ghamdi, S.G. (2018). Reducing electric energy consumption in linear fresnel collector solar fields coupled to thermal desalination plants by optimal mirror defocusing. *Heliyon*, 4(9), e00813.

Bermejo, P., Pino, F.J., and Rosa, F. (2010). Solar absorption cooling plant in seville. *Solar Energy*, 84(8), 1503–1512.

Camacho, E.F., Berenguel, M., and Gallego, Antonio, J. (2014). Control of thermal solar energy plants. *Journal of Process Control*, 24(2), 332 – 340. ADCHEM 2012 Special Issue.

Correa-Jullian, C., Cardemil, J.M., López Droguett, E., and Behzad, M. (2020). Assessment of deep learning techniques for prognosis of solar thermal systems. *Renewable Energy*, 145, 2178 – 2191.

Faure, G., Vallée, M., Tran-Quoc, T., Lamaison, N., and Paulus, C. (2018). A methodology to analyse fault effect on large solar thermal system behaviour.

Faure, G., Vallée, M., Paulus, C., and Tran, Q. (2016). Reviewing the dysfunctions of large solar thermal system: a classification of sub-systems reliability. In *ISES Conference Proceedings*.

Fine, T.L. (2006). *Feedforward neural network methodology*. Springer Science & Business Media.

Freire, V.A., Márquez, J.J., Bordons, C., Zafra-Cabeza, A., and de Arruda, L.V.R. (2020). Energy management system for microgrid considering operational faults in power supply. In *2020 International Conference on Smart Energy Systems and Technologies (SEST)*, 1–6.

Gallego, A.J., Sánchez, A.J., Berenguel, M., and Camacho, E.F. (2020). Adaptive ukf-based model predictive control of a fresnel collector field. *Journal of Process Control*, 85, 76 – 90.

Gallego, Antonio, J., Merello, G.M., Berenguel, M., and Camacho, E.F. (2019). Gain-scheduling model predictive control of a fresnel collector field. *Control Engineering Practice*, 82, 1 – 13.

Goswami, D.Y., Kreith, F., and Kreider, J.F. (2000). *Principles of solar engineering*. CRC Press.

Islam, M.T., Huda, N., Abdullah, A.B., and Saidur, R. (2018). A comprehensive review of state-of-the-art concentrating solar power (csp) technologies: Current status and research trends. *Renewable and Sustainable Energy Reviews*, 91, 987–1018.

Jiang, S., Lian, M., Lu, C., Ruan, S., Wang, Z., and Chen, B. (2019). Svm-ds fusion based soft fault detection and diagnosis in solar water heaters. *Energy Exploration & Exploitation*, 37(3), 1125–1146.

Kalogirou, S., Lalot, S., Florides, G., and Desmet, B. (2008). Development of a neural network-based fault diagnostic system for solar thermal applications. *Solar Energy*, 82(2), 164 – 172.

Kim, D. and Infante Ferreira, C. (2008). Solar refrigeration options – a state-of-the-art review. *International Journal of Refrigeration*, 31(1), 3–15.

Lillicrap, T.P., Santoro, A., Marris, L., Akerman, C.J., and Hinton, G. (2020). Backpropagation and the brain. *Nature Reviews Neuroscience*, 21(6), 335–346.

McCulloch, W.S. and Pitts, W. (1943). A logical calculus of the ideas immanent in nervous activity. *The bulletin of mathematical biophysics*, 5(4), 115–133.

NREL (2022a). Liddell power station CSP project, feb 2022, https://solarpaces.nrel.gov/project/liddell-power-station.

NREL (2022b). Puerto errado 2 thermosolar power plant CSP project, feb 2022, https://solarpaces.nrel.gov/project/puerto-errado-2-thermosolar-power-plant.

Pillai, D.S., Blaabjerg, F., and Rajasekar, N. (2019). A comparative evaluation of advanced fault detection approaches for pv systems. *IEEE Journal of Photovoltaics*, 9(2), 513–527.

Pulido-Iparraguirre, D., Valenzuela, L., Serrano-Aguilera, J.J., and Fernández-García, A. (2019). Optimized design of a linear fresnel reflector for solar process heat applications. *Renewable Energy*, 131, 1089–1106.

Qu, F., Liu, J., Liu, X., and Jiang, L. (2021). A multi-fault detection method with improved triplet loss based on hard sample mining. *IEEE Transactions on Sustainable Energy*, 12(1), 127–137.

Robledo, M., Escaño, J.M., Núñez, A., Bordons, C., and Camacho, E.F. (2011). Development and experimental validation of a dynamic model for a fresnel solar collector. *IFAC Proceedings Volumes*, 44(1), 483–488. 18th IFAC World Congress.

Rumelhart, D.E., Hinton, G.E., and Williams, R.J. (1986). Learning representations by back-propagating errors. *nature*, 323(6088), 533–536.

Rungasamy, A., Craig, K., and Meyer, J. (2021). A review of linear fresnel primary optical design methodologies. *Solar Energy*, 224, 833–854.

Sánchez, A.J., Gallejo, A.J., Escaño, J.M., and Camacho, E.F. (2020). Parabolic trough collector defocusing analysis: Two control stages vs four control stages. *Solar Energy*, 209, 30 – 41.

Whitheephanich, K., Escaño, J.M., Len, A.J., and Camacho, E.F. (2013). Pressurized water temperature control of a fresnel collector field-type solar cooling system using explicit model predictive control.

Zahra, T., Mourad, L.M., and Ahmed, A.H. (2020). Robust fuzzy sliding mode observer for faults detection in solar power plant application. *Instrumentation, Mesures, Métrologies*, 19(4).